

Article

Control of Carrier Concentration by Ag Doping in N-Type Bi₂Te₃ Based Compounds

Jae Ki Lee ¹, Ji Hui Son ¹, Yong-Il Kim ², Byungki Ryu ¹, Byung Jin Cho ³, Sookyung Kim ⁴,
Su-Dong Park ¹ and Min-Wook Oh ^{5,*} 

¹ Thermoelectric Conversion Research Center, Korea Electrotechnology Research Institute, Changwon 51543, Korea; jackyrhy@gmail.com (J.K.L.); jhson@keri.re.kr (J.H.S.); byungkiryu@keri.re.kr (B.R.); john@keri.re.kr (S.D.P.)

² Center for Convergence Property Measurement, Korea Research Institute of Standards and Science (KRISS), Daejeon 34113, Korea; yikim@kriss.re.kr

³ Department of Electrical Engineering, KAIST, Daejeon 34141, Korea; elebjcho81@kaist.ac.kr

⁴ Mineral Resources Division, Korea Institute of Geoscience and Mineral Resources, Daejeon 34132, Korea; skkim@kigam.re.kr

⁵ Department of Materials Science and Engineering, Hanbat National University, Daejeon 31458, Korea

* Correspondence: mwoh@hanbat.ac.kr; Tel.: +82-42-821-1247

Received: 30 March 2018; Accepted: 3 May 2018; Published: 6 May 2018



Abstract: Many elements have been used as dopants to enhance the thermoelectric performance of Bi₂Te₃-related materials. Among them, Ag's effect on thermoelectric properties, where Ag acts as a donor or acceptor, remains unclear. To elucidate the role of Ag in n-type Bi₂Te₃ based compounds, Ag was added to n-type (Bi_{0.9}Sb_{0.1})₂(Te_{0.85}Se_{0.15})₃. As the amount of Ag was increased, the electron concentration decreased, which means Ag acted as an acceptor. The added Ag atoms were found to occupy interstitial sites in the hexagonal lattices, as confirmed by X-ray analysis and first principles calculations. The reduction in electron concentration was attributed to the interaction between the interstitial Ag and intrinsic defects.

Keywords: thermoelectric; Bi₂Te₃; Ag; defects; carrier concentration

1. Introduction

Thermoelectric materials have excellent potential to improve levels of global energy consumption by using recovered waste heat to generate power, and enabling all solid-state refrigeration technology [1,2]. To realize this potential, thermoelectric materials are needed which have a large value of the dimensionless figure of merit, $ZT = (\alpha^2/\rho\kappa) T$, where α , ρ , κ , and T are the Seebeck coefficient, electrical resistivity, thermal conductivity, and absolute temperature, respectively [1]. Bi₂Te₃-based compounds have been widely used for room temperature applications, and many studies have been performed in efforts to improve their ZT [3–11]. Strategies to achieve large ZT have mainly focused on two schemes: (a) enhancing the power factor ($PF = \alpha^2/\rho$); and (b) reducing phonon thermal conductivity (κ_ρ). However, before attempting to enhance PF with novel technologies such as nanostructures and band structure engineering, the carrier concentration should be optimized. Appropriate control of carrier concentration is one of the prerequisites for achieving enhanced ZT .

Doping is one of the routes that can be used to control carrier concentration. The full or partial ionization of donor and acceptor dopants creates electrons and holes, respectively. As examples, Fe was substituted for Bi as a donor type dopant [9,12], while Pb has been substituted for Bi as an acceptor [13]. Interstitial Cu acted as the donors in Bi₂Te₃ [14,15].

Among the many studies on dopants in Bi₂Te₃, the effects of Ag on the transport properties of Bi₂Te₃-based materials have been frequently reported. Park et al. reported that the addition of

Ag (0.01–0.2 wt %) decreased electrical resistivity and the Seebeck coefficient, an effect which they attributed to the Ag particles, which did not substitute for Bi or Sb [16]. Lee et al. reported that ρ and α decreased with Ag, which substituted for Bi or Sb in p-type $(\text{Bi,Sb})_2\text{Te}_3$ [17]. The substitution of Ag for Bi or Sb was also reported by Klichová et al. [18]. All of these results said that the Ag acted as an acceptor in the p-type $(\text{Bi,Sb})_2\text{Te}_3$ compounds.

For n-type Bi_2Te_3 , a different Ag behavior has been reported. Navrátil et al. found that interstitial Ag was formed in n-type Bi_2Te_3 and behaved as a donor, while Ag behaved as an acceptor in Sb_2Te_3 [19]. Yang et al. reported that interstitial Ag formed in n-type $\text{Bi}_2(\text{Te,Se})_3$ and acted as an n-type donor when Ag content was less than 0.2 wt %, and like a p-type acceptor at higher Ag content (> 0.2 wt %) [20]. However, both studies deduced the existence of interstitial Ag by investigating electrical transport properties, and there was no direct evidence to confirm that interstitial Ag formed in the Bi_2Te_3 unit cell. They noted that electrical conductivity and electron concentration increased after the addition of Ag to n-type Bi_2Te_3 and then they argued that the electrons were donated by the interstitial Ag. Lu et al. reported that even though interstitial Ag was formed in the n-type $\text{Bi}_2(\text{Te,Se})_3$, the electron concentration was reduced when Ag content was less than 0.5 wt %, while the concentration increased with higher Ag content (> 0.5 wt %) [21]. Controversy about the effect of Ag in n-type $\text{Bi}_2(\text{Te,Se})_3$ has arisen; low Ag content has been reported to reduce electron concentration [21] and to increase electron concentration [20]. Accordingly, we think that the location of Ag in the Bi_2Te_3 unit cell, and the effect of Ag on the electrical transport properties, have not been clearly demonstrated.

In this study, Ag was added to n-type $\text{Bi}_2(\text{Te,Se})_3$ and the effect of the Ag addition on the carrier concentration was investigated. With both experimental and theoretical investigations, we tried to establish whether Ag occupies a position in the Bi_2Te_3 unit cell and acts as an acceptor or donor. We also focused on new findings, that the dopant can control the concentration of native defects in Bi_2Te_3 , and that the dopant can donate carriers through ionization.

2. Materials and Methods

Commercial 99.999% high purity elements of Bi, Sb, Te, Se, and 99.99% Ag were weighed according to the stoichiometry of $(\text{Bi}_{0.9}\text{Sb}_{0.1})_2(\text{Te}_{0.85}\text{Se}_{0.15})_3 + \text{Ag}$. The amounts of added Ag were chosen to be 0, 0.005, 0.01, 0.03, 0.05 wt %. Sb and Se were added to Bi_2Te_3 , because we wished to investigate the effect of Ag on the transport properties of compounds that were close to the conventionally used composition [22]. The mixed elements were loaded into quartz tubes and sealed under Ar atmosphere. Using a rocking furnace, the mixtures were heated to 1073 K for 10 h. After water quenching, the ingots were crushed by ball milling for 2 h under Ar atmosphere to prevent oxidation. The powders were sintered at 693 K for 30 min at a pressure of 200 MPa using a hot press, and obtained n-type Bi_2Te_3 bulk materials. These bulk materials were analyzed by X-ray diffraction (X'pert, Malvern Panalytical, Almero, the Netherlands) using Cu K α radiation ($\lambda = 0.15406$ nm) to determine their crystal structure. Their electrical conductivity and Seebeck coefficient were measured using ZEM-3 (Ulvac-Riko, Yokohama, Japan). The carrier concentration was measured by the Hall effect at room temperature under 0.55T (HMS-3000, ECOPIA, Anyang, Korea). The first-principles calculations were performed using the Vienna ab initio simulation package (VASP) code [23,24]. A supercell containing 60 atoms in a hexagonal cell was used to evaluate the formation energy of defects and Ag occupation. A plane wave cutoff of 350 eV and a k-point mesh grid of $7 \times 7 \times 2$ were used to ensure energy convergence [7]. The van der Waals interaction set out by Tkatchenko and Scheffler within GGA was used in the structural optimization [25,26].

3. Results and Discussions

Figure 1a shows the temperature dependence of the electrical resistivity and the Seebeck coefficient. The negative Seebeck coefficient indicates that the major carriers are electrons. As the amount of Ag is increased, the value of the electrical resistivity is increased. The absolute value of the Seebeck coefficient increased with Ag content. Both the increases in electrical resistivity and Seebeck coefficient

with Ag may be attributed to a reduction in carrier concentration, because the electrical resistivity and the Seebeck coefficient are approximately proportional to n^{-1} and $n^{-2/3}$, respectively [1]; this will be also supported by the measurement of the Hall coefficient.

A reduction in electron concentration is responsible for an increase in electrical resistivity and Seebeck coefficient, which is generally acceptable for the transport properties within the considered carrier concentration in the Bi_2Te_3 -related compounds [27].

The power factor (α^2/σ) is shown in Figure 1b. It is well known that the values are dependent on the carrier concentration and show maximum values at the optimized concentration [1]. The maximum value of 1.73 mW/mK^2 was achieved in the 0.01 wt % Ag sample.

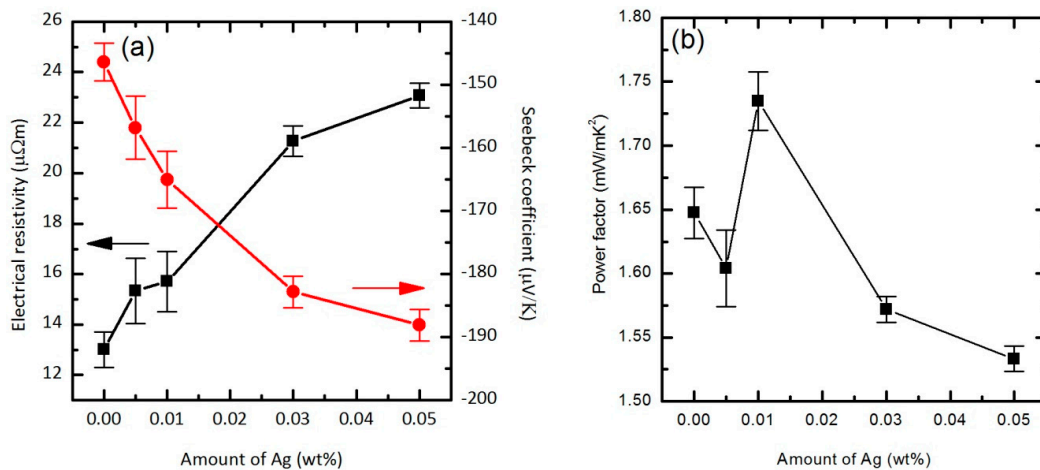


Figure 1. The variation in electrical resistivity, Seebeck coefficient and power factor at room temperature with respect to the amount of Ag: (a) the electrical resistivity and Seebeck coefficient and (b) the power factor.

Figure 2 shows the carrier concentration of samples as determined from the Hall coefficient (R_H) measurement. All of the Hall coefficient values were negative, which means electrons were the dominant carriers. The electron concentrations were evaluated using $R_H = 1/ne$, where n is the electron concentration and e is the charge of the electrons. As the amount of Ag increased, the electron concentrations decreased. Thus, the increases in electrical resistivity and Seebeck coefficient are due to the reduction in carrier concentration with Ag.

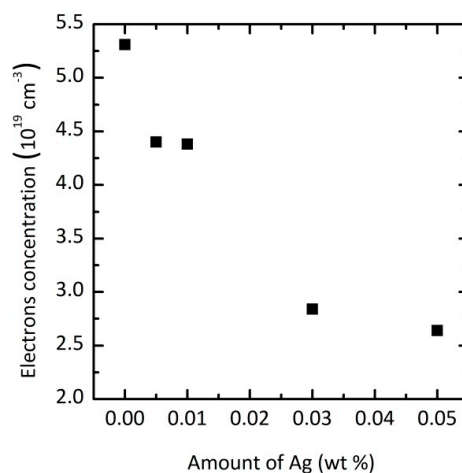


Figure 2. Electron concentrations estimated from Hall coefficient as a function of Ag amount.

In order to understand the origin of this reduction in electron concentrations, changes in the crystal structure that occurred with Ag doping were analyzed. Figure 3 shows the observed XRD and Rietveld refinement patterns of Bi_2Te_3 , and the refined structural parameters are shown in Table 1 [28]. Even though Bi, Sb, Te, and Se atoms exist at the lattice sites, a refinement was performed for the hexagonal $R\text{-}3m$ structure with Bi in the 6c (0, 0, z(Bi)) sites, Te(1) in the 3a (0, 0, 0) sites, and Te(2) in the 6c (0, 0, z(Te)) sites. The refined lattice parameters of both the a and c axes were smaller than those of Bi_2Te_3 , and this was attributed to the small amounts of Sb and Se substituted for Bi and Te, respectively. Because the covalent radius of Sb (139 pm) and Se (120 pm) is smaller than that of Bi (148 pm) and Te (138 pm), respectively, the lattice parameters will be decreased with Se [29].

The lattice parameters of the Ag-doped samples were also obtained with a Rietveld refinement and the results are shown in Table 2. The lattice parameters of the c-axis significantly increased with Ag, while the values of the a-axis were nearly the same. It should be noted that the covalent radius of Bi is significantly larger than that of Ag, resulting in a reduction of the lattice parameter if Ag is substituted for Bi. Thus, this anisotropic change and the increase in the lattice parameters indicate that Ag was not substituted for Bi. It is believed that Ag is located at the interstitial sites (0, 0, 0.5 in fractional coordinates) which are also known as van der Waals gaps, due to van der Waals bonding character between Te(2) and Te(2) atoms.

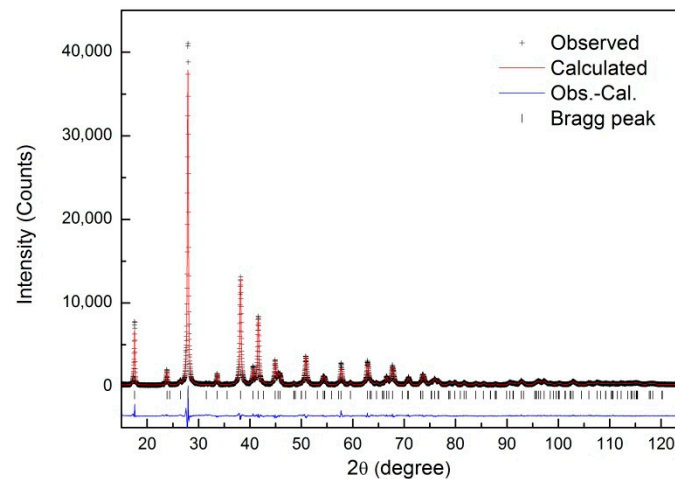


Figure 3. Rietveld refinement patterns of heat-treated Bi_2Te_3 sample using X-ray powder diffraction data. Plus marks (+) represent the observed intensities, and the red solid line is the calculated result. The difference plot (blue) is shown at the bottom. Tick marks above the difference plot indicate the reflection positions.

Table 1. Refined structural parameters of heat-treated Bi_2Te_3 sample obtained from the Rietveld refinement using X-ray powder diffraction data at 297 K. The symbol, g, is the occupation factor. The numbers in parentheses are the estimated standard deviations of the last significant figure.

Atom	site	x/a	y/b	z/c	g	$B_{\text{eq}}/\text{\AA}^2$
Te(1)	3a	0	0	0	1.0	1.86(1)
Te(2)	6c	0	0	0.7885(1)	1.0	1.36(7)
Bi(1)	6c	0	0	0.3984(1)	1.0	1.37(5)

Space group: $R\text{-}3m$ (no. 166) and $Z = 3$; $a (= b) = 4.3377(1) \text{ \AA}$, $c = 30.2611(1) \text{ \AA}$; $\alpha = \beta = 90^\circ$, $\gamma = 120^\circ$; R -factor: $R_{\text{wp}} = 8.44$, $R_{\text{p}} = 6.49$, $R_{\text{e}} = 3.95$ and $S (= R_{\text{wp}}/R_{\text{e}}) = 2.14$.

Table 2. Refined lattice parameters and R-weighted factors (R_{wp}) for the heat-treated Bi_2Te_3 and heat-treated Ag doped Bi_2Te_3 samples obtained from the Rietveld refinement using X-ray powder diffraction data at 297 K.

Sample	R_{wp} (%)	a (Å)	c (Å)
Ag = 0.0	8.44	4.3377(1)	30.2611(1)
Ag = 0.01	8.61	4.3375(1)	30.2641(1)
Ag = 0.03	7.82	4.3380(1)	30.2768(1)
Ag = 0.05	7.97	4.3387(1)	30.2774(1)

In order to elucidate the Ag interstitial occupation, the formation energy of Ag in Bi_2Te_3 and its structural properties were evaluated using first-principles calculations. The lattice parameters and the formation energy obtained from the first-principles calculations are shown in Table 3. The only increase in the lattice parameter of the c-axis was for Ag-interstitial (Ag_i), while this value decreased for the other models. It is fairly difficult to compare the absolute value of the differences in the lattice parameters with the experimental calculations, because the amount of Ag in the modeled alloys is much larger than that in the experiment. The results of the formation energy also support Ag_i in Bi_2Te_3 . The lowest energy of formation was obtained for Ag_i .

Table 3. The optimized lattice parameters and formation energy from the first-principles calculation. The values of pristine Bi_2Te_3 , Ag interstitial (Ag_i)-doped Bi_2Te_3 , Bi_2Te_3 with Ag substituted for Bi (Ag_{Bi}), and Bi_2Te_3 with Ag substituted for Te sites (6c and 3a) are listed.

Sample	Lattice Parameters (Å)		Formation Energy (eV)	
	a	c	Te-Rich	Bi-Rich
Bi_2Te_3	4.421	30.478	-	-
Ag_i	4.443	30.660	0.68	0.68
Ag_{Bi}	4.408	30.211	1.07	1.47
$\text{Ag}_{\text{Te}(6c)}$	4.422	30.046	1.83	1.57
$\text{Ag}_{\text{Te}(3a)}$	4.415	30.323	1.89	1.63

From the results of the lattice parameters and the first-principles calculations, it may be thought that the reduction in electron concentrations is due to the Ag-interstitial. However, it can be expected that metal atoms at the interstitial site will donate electrons, following the reaction equation



where Ag_s means solid and nonactivated Ag atoms. Accordingly, if Ag is interstitial, electron concentrations should increase with Ag, which is contrary to the results of the transport properties.

To understand the mechanism for the change in carrier concentration with Ag addition, we then considered the intrinsic defects, because the carrier concentrations in Bi_2Te_3 related compounds are mainly determined by such defects. For n-type transport properties, it is known that the n-type Te_{Bi} antisite defects (Te at Bi sites) are the first major defects, and the second major defects are the n-type vacancies of Te (V_{Te}) [7,30–32]. Because the concentration of antisite defects is highly dependent on the average difference in electronegativity between cations and anions [7,9], in Bi_2Te_3 dopants such as In and Pb interact with the native defects, and this changes the concentration of the defects [9,13,33].

It was thought that the addition of Ag might also interact with the antisite defects or vacancies, resulting in a reduction in electron concentration. We subsequently confirmed the interaction of Ag with the defects. The Te metal phase in the samples with Ag was clearly observed in SEM images, as shown in Figure 4. The interaction of Ag with Te_{Bi} decreased the concentration of Te_{Bi} so that the remaining Te, which could not be included in the lattice, was then expelled as a metal phase.

However, it is also important to consider the possibility of interaction between the Ag interstitials and V_{Te} . Lu et al. reported that interstitial Ag might increase the formation energy of V_{Te} and suppress the formation of V_{Te} and in turn electron concentration was decreased [21]. The reactions between Ag_i and the defects are proposed below



The coefficients of x and y indicate how efficiently the formation of Te_{Bi} and V_{Te} was suppressed by Ag_i [21].

The interaction of Ag and antisite defects was investigated using the formation energy obtained from the first-principles calculations in Figure 5. In the formation energy calculations, we only considered antisite defects because the calculations always confirmed that antisite defects were the major defects. The absolute values of Te_{Bi} and Bi_{Te} decreased with Ag. The relative reduction in energy after the incorporation of Ag_i was larger in Bi_{Te} than that in Te_{Bi} : the reduction was 0.71 and 0.59 eV for Bi_{Te} and Te_{Bi} , respectively, which means that Ag_i stabilized Bi_{Te} as compared with Te_{Bi} . The major defect in the Te-rich condition was Te_{Bi} , regardless of Ag_i . However, the chemical potential of Te (μ_{Te}) varied with dopants such as Sb and Se, and fabrication condition. The μ_{Te} region between 0 eV (Te metal) and the cross point of the two lines of Te_{Bi} and Bi_{Te} means that Te_{Bi} is more preferred than Bi_{Te} . It should be noted that the region decreased with Ag_i . Therefore, we also confirmed that Ag_i acts as a stabilizer of Bi_{Te} .

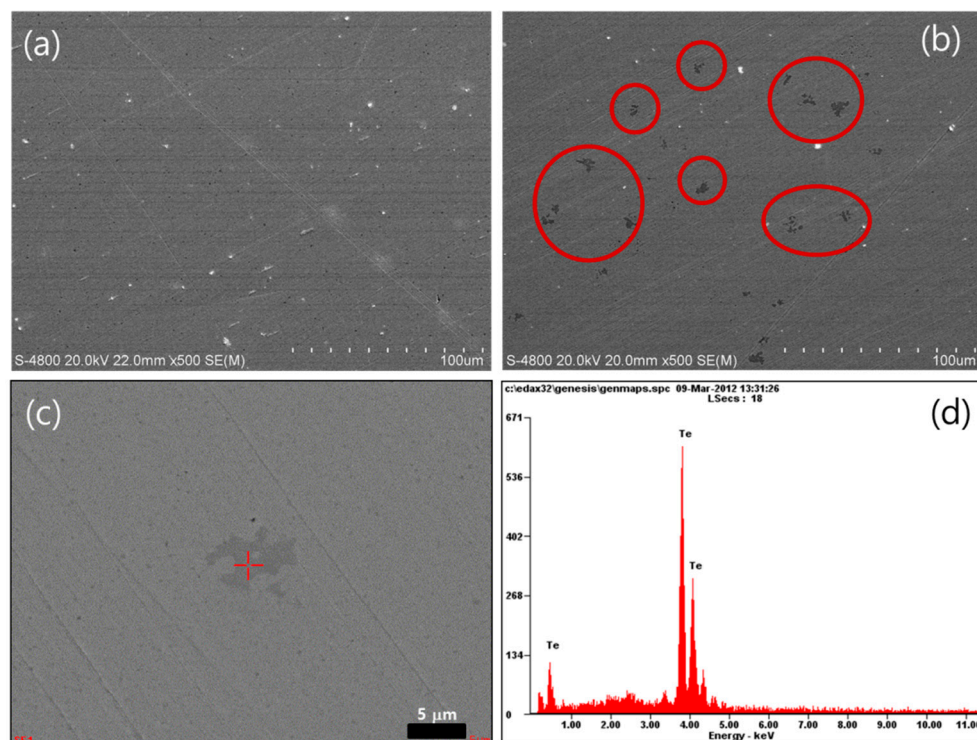


Figure 4. SEM images of the n-type samples (a) without Ag; (b) with 0.05 wt % Ag; (c) and (d) are the SEM image used in the EDS composition analysis, and the spectrum obtained from the spot in (c), respectively.

In p-type Bi_2Te_3 , it was reported that Ag was substituted for Bi or Sb, which is contrary to the results in this study. The difference in the position occupied by Ag between p- and n-type Bi_2Te_3 is possibly due to the lattice parameters. The c-axis lattice parameters of the p-type are significantly

smaller than that of the n-type, because the covalent radius of Sb is smaller than that of Bi, and 75% Sb_2Te_3 is added to Bi_2Te_3 for p-type transport. Thus, Ag needs more energy to enlarge the unit cell to occupy the interstitial position in the smaller unit cell. We confirmed that the formation energy of Ag_{Bi} ranged from 1.09 to 1.07 eV as the c-axis varied from 30.468 to 30.497 Å, whereas the energy of Ag_i ranged from 1.48 to 1.45 eV. Even though Ag_i is more stable in the enlarged cell, Ag_{Bi} is more preferred than Ag_i in the reduced cell.

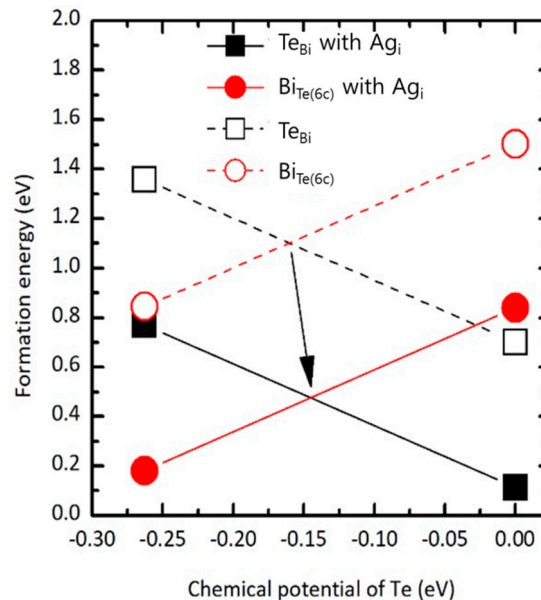


Figure 5. Formation energy of the defects in Bi_2Te_3 as a function of the Te chemical potential. The antisite defects with Ag_i (interstitial Ag) and without Ag_i were considered. The chemical potential of metal Te was set to be 0 eV.

4. Conclusions

In summary, the variation in carrier concentration with Ag addition in n-type Bi_2Te_3 was examined by various measurements including electrical resistivity, the Seebeck coefficient, and the Hall coefficient. The electron concentrations in n-type Bi_2Te_3 decreased with Ag addition. The Ag atoms occupied interstitial positions in the Bi_2Te_3 unit cell. It was confirmed that Ag did not directly induce the change in carrier concentration by its ionization, but by affecting the formation of defects. The carrier concentration was determined by the interaction between Ag and the defects.

Author Contributions: M.W.O., B.R., S.K.K., and S.D.P. conceived and designed the experiments; J.H.S. performed the transport properties measurement and preparation of materials; B.R. contributed to calculations; J.K.L., M.W.O., and B.J.C. analyzed the data; Y.I.K. performed X-ray analysis; J.K.L. and M.W.O. contributed to the paper writing.

Acknowledgments: This research was supported by the research fund of a National Research Foundation of Korea (NRF) grant funded by the Korean Government (NRF-2015R1A5A1036133).

Conflicts of Interest: The authors declare no conflict of interest.

References

1. Snyder, G.J.; Toberer, E.S. Complex thermoelectric materials. *Nat. Mater.* **2008**, *7*, 105–114. [[CrossRef](#)] [[PubMed](#)]
2. Sales, B.C. Smaller Is Cooler. *Science* **2002**, *295*, 1248–1249. [[CrossRef](#)] [[PubMed](#)]
3. Poudel, B.; Hao, Q.; Ma, Y.; Lan, Y.; Minnich, A.; Yu, B.; Yan, X.; Wang, D.; Muto, A.; Vashaee, D.; et al. High-Thermoelectric Performance of Nanostructured Bismuth Antimony Telluride Bulk Alloys. *Science* **2008**, *320*, 634–638. [[CrossRef](#)] [[PubMed](#)]

4. Seo, S.; Jeong, Y.; Oh, M.W.; Yoo, B. Effect of hydrogen annealing of ball-milled Bi_{0.5}Sb_{1.5}Te₃ powders on thermoelectric properties. *J. Alloys Compd.* **2017**, *706*, 576–583. [[CrossRef](#)]
5. Seo, S.; Oh, M.W.; Jeong, Y.; Yoo, B. A hybrid method for the synthesis of small Bi_{0.5}Sb_{1.5}Te₃ alloy particles. *J. Alloys Compd.* **2017**, *696*, 1151–1158. [[CrossRef](#)]
6. Kim, S.J.; Choi, H.; Kim, Y.; We, J.H.; Shin, J.S.; Lee, H.E.; Oh, M.W.; Lee, K.J.; Cho, B.J. Post ionized defect engineering of the screen-printed Bi₂Te_{2.7}Se_{0.3} thick film for high performance flexible thermoelectric generator. *Nano Energy* **2017**, *31*, 258–263. [[CrossRef](#)]
7. Oh, M.W.; Son, J.H.; Kim, B.S.; Park, S.D.; Min, B.K.; Lee, H.W. Antisite defects in n-type Bi₂(Te, Se)₃: Experimental and theoretical studies. *J. Appl. Phys.* **2014**, *115*, 133706. [[CrossRef](#)]
8. Seo, S.; Lee, K.; Jeong, Y.; Oh, M.W.; Yoo, B. Method of efficient Ag doping for Fermi level tuning of thermoelectric Bi_{0.5}Sb_{1.5}Te₃ alloys using a chemical displacement reaction. *J. Phys. Chem. C* **2015**, *119*, 18038–18045. [[CrossRef](#)]
9. Son, J.H.; Oh, M.W.; Kim, B.S.; Park, S.D.; Min, B.K.; Kim, M.H.; Lee, H.W. Effect of ball milling time on the thermoelectric properties of p-type (Bi,Sb)₂Te₃. *J. Alloys Compd.* **2013**, *566*, 168–174. [[CrossRef](#)]
10. Ryu, B.; Oh, M.W. Computational Simulations of Thermoelectric Transport Properties. *J. Korean Ceram. Soc.* **2016**, *53*, 273–281. [[CrossRef](#)]
11. Lee, K.H.; Kim, S.W. Design and Preparation of High-Performance Bulk Thermoelectric Materials with Defect Structures. *J. Korean Ceram. Soc.* **2017**, *54*, 75–85. [[CrossRef](#)]
12. Kulbachinskii, V.A.; Kaminskii, A.Y.; Kindo, K.; Narumi, Y.; Suga, K.; Lostak, P.; Svanda, P. Ferromagnetism in new diluted magnetic semiconductor Bi_{2-x}Fe_xTe₃. *Physica B* **2002**, *311*, 292–297. [[CrossRef](#)]
13. Plecháček, T.; Navrátil, J.; Horák, J.; Lošťák, P. Defect structure of Pb-doped Bi₂Te₃ single crystals. *Philos. Mag.* **2004**, *84*, 2217–2228. [[CrossRef](#)]
14. Han, M.K.; Ahn, K.; Kim, H.J.; Rhyee, J.S.; Kim, S.J. Formation of Cu nanoparticles in layered Bi₂Te₃ and their effect on ZT enhancement. *J. Mater. Chem.* **2011**, *21*, 11365–11370. [[CrossRef](#)]
15. Liu, W.S.; Zhang, Q.; Lan, Y.; Chen, S.; Yan, X.; Zhang, Q.; Wang, H.; Wang, D.; Chen, G.; Ren, Z. Thermoelectric property studies on Cu-doped n-type Cu_xBi₂Te_{2.7}Se_{0.3} nanocomposites. *Adv. Energy Mater.* **2011**, *1*, 577–587. [[CrossRef](#)]
16. Park, Y.H.; Liu, X.D. Thermoelectric Properties of Bi-Sb-Te-X Compounds Prepared by MA-PDS Method. *Mater. Res. Soc. Symp. Proc.* **2002**, *691*. [[CrossRef](#)]
17. Lee, J.K.; Park, S.D.; Kim, B.S.; Oh, M.W.; Cho, S.H.; Min, B.K.; Lee, H.W.; Kim, M.H. Control of thermoelectric properties through the addition of Ag in the Bi_{0.5}Sb_{1.5}Te₃ alloy. *Electron. Mater. Lett.* **2010**, *6*, 201–207. [[CrossRef](#)]
18. Klichová, I.; Lošťák, P.; Drašar, Č.; Navrátil, J.; Beneš, L.; Šrámková, J. Characterization of Ag-doped Sb_{1.5}Bi_{0.5}Te₃ single crystals. *Radiat. Eff. Defects Solids* **1998**, *145*, 245–262. [[CrossRef](#)]
19. Navrátil, J.; Klichová, I.; Karamazov, S.; Šrámková, J.; Horák, J. Behavior of Ag Admixtures in Sb₂Te₃ and Bi₂Te₃ Single Crystals. *J. Solid State Chem.* **1998**, *140*, 29–37. [[CrossRef](#)]
20. Yang, J.; Chen, R.; Fan, X.; Bao, S.; Zhu, W. Thermoelectric properties of silver-doped n-type Bi₂Te₃-based material prepared by mechanical alloying and subsequent hot pressing. *J. Alloys Compd.* **2006**, *407*, 330–333. [[CrossRef](#)]
21. Lu, M.P.; Liao, C.N.; Huang, J.Y.; Hsu, H.C. Thermoelectric Properties of Ag-Doped Bi₂(Se,Te)₃ Compounds: Dual Electronic Nature of Ag-Related Lattice Defects. *Inorg. Chem.* **2015**, *54*, 7438–7444. [[CrossRef](#)] [[PubMed](#)]
22. Nolas, G.S.; Sharp, J.; Goldsmid, J. *Thermoelectrics: Basic Principles and New Materials Developments*, 1st ed.; Springer: Heidelberg, Germany, 2001; pp. 111–131. ISBN 3-540-41245-X.
23. Kresse, G.; Hafner, J. Ab initio molecular dynamics for liquid metals. *Phys. Rev. B* **1993**, *47*, R558. [[CrossRef](#)]
24. Kresse, G.; Hafner, J. Ab initio molecular-dynamics simulation of the liquid-metal-amorphous-semiconductor transition in germanium. *Phys. Rev. B* **1994**, *49*, 14251. [[CrossRef](#)]
25. Tkatchenko, A.; Scheffler, M. Accurate Molecular Van Der Waals Interactions from Ground-State Electron Density and Free-Atom Reference Data. *Phys. Rev. Lett.* **2009**, *102*, 073005. [[CrossRef](#)] [[PubMed](#)]
26. Perdew, J.P.; Burke, K.; Ernzerhof, M. Generalized Gradient Approximation Made Simple. *Phys. Rev. Lett.* **1996**, *77*, 3865. [[CrossRef](#)] [[PubMed](#)]
27. Scherrer, H.; Scherrer, S. *CRC Handbook of Thermoelectrics*, 1st ed.; Rowe, D.M., Ed.; CRC Press: Boca Raton, FL, USA, 1995; pp. 211–237. ISBN 0-8493-0146-7.

28. Toby, B.H. EXPGUI, a graphical user interface for GSAS. *J. Appl. Crystallogr.* **2001**, *34*, 210–213. [[CrossRef](#)]
29. Cordero, B.; Gómez, V.; Platero-Prats, A.E.; Revés, M.; Echeverria, J.; Cremades, E.; Barragán, F.; Alvarez, S. Covalent radii revisited. *Dalton Trans.* **2008**, *21*, 2832. [[CrossRef](#)] [[PubMed](#)]
30. Hashibon, A.; Elsässer, C. First-principles density functional theory study of native point defects in Bi₂Te₃. *Phys. Rev. B* **2011**, *84*, 144117. [[CrossRef](#)]
31. West, D.; Sun, Y.Y.; Wang, H.; Bang, J.; Zhang, S.B. Native defects in second-generation topological insulators: Effect of spin-orbit interaction on Bi₂Se₃. *Phys. Rev. B* **2012**, *86*, 121201(R). [[CrossRef](#)]
32. Wang, L.L.; Huang, M.; Thimmaiah, S.; Alam, A.; Bud'ko, S.L.; Kaminski, A.; Lograsso, T.A.; Canfield, P.; Johnson, D.D. Native defects in tetradymite Bi₂(Te_xSe_{3-x}) topological insulators. *Phys. Rev. B* **2013**, *87*, 125303. [[CrossRef](#)]
33. Horák, J.; Čermák, K.; Koudelka, L. Energy formation of antisite defects in doped Sb₂Te₃ and Bi₂Te₃ crystals. *J. Phys. Chem. Solids* **1986**, *47*, 805. [[CrossRef](#)]



© 2018 by the authors. Licensee MDPI, Basel, Switzerland. This article is an open access article distributed under the terms and conditions of the Creative Commons Attribution (CC BY) license (<http://creativecommons.org/licenses/by/4.0/>).